Advanced Biomedical Engineering
13: 11–18, 2024.

Original Paper

DOI:10.14326/abe.13.11

Raman Spectroscopic Evaluation of Composition of Matrix Synthesized by Osteoblasts under Microvibration Stimulation

Katsuya Sato,[*,#] Takeo Minamikawa,[**] Takeshi Yasui[**]

Abstract In this study, we used Raman spectroscopy to observe the process of osteoblast calcification under microvibration stimulation. Osteoblast cultures were prepared under three conditions: the control group was cultured statically without vibration stimulation, and the 45-Hz vibration group and 90-Hz vibration group were stimulated by microvibration at 45 Hz and 90 Hz, respectively, for 30 minutes per day with an acceleration amplitude of 0.2 G. The incubation periods were 7, 9, 11 and 14 days, and observations were conducted using Raman spectroscopy after fixation. In the 45-Hz vibration group, calcification was accelerated. This group produced a large amount of highly crystalline phosphate with large crystal size and a low proportion of hyaluronan precursor and carbonate. In the 90-Hz vibration group, differentiation into mature osteoblasts was not rapid. This group produced more non-crystalline phosphate containing more hyaluronan precursors and carbonate than the other groups. The results suggest that microvibration stimulation promotes calcification, and that the composition of the calcified area may differ depending on the vibration conditions.

Keywords: osteoblast, vibration stimuli, cell biomechanics, calcified matrix, Raman spectroscopy.

Adv Biomed Eng. **13**: pp. 11–18, 2024.

1. Introduction

In bone tissue, osteoclasts constantly resorb old bone matrix, and osteoblasts synthesize new bone matrix to replace it. This metabolic activity is called bone remodeling, and an imbalance in bone remodeling is one of the causes of osteoporosis. Osteoporosis is a disease characterized by a decrease in bone mass and deterioration of the microstructure of bone tissue, and is known to increase the risk of fracture as a result of increased bone fragility [1]. Osteoporosis induces bone fractures due to falls, etc., and is a factor that decreases the quality of life of the elderly [2, 3]. Osteoporosis is one of the most important diseases in the aging society. Currently, estrogen replacement therapy and alendronate therapy are used as pharmacological treatments for osteoporosis. However, estrogen replacement therapy has adverse effects such as risk of breast cancer [4], and alendronate therapy has adverse effects such as esophageal and oral disorders [5]. Therefore, non-pharmacological methods including physical exercise and strength training are used in combination with alendronate therapy to reduce adverse effects by controlling the dosage of drugs.

Bone is known to adjust its mass and microstructure in response to the demands of mechanical loading [6]. Mechanical signals such as force or deformation stimulate bone formation and reduce bone resorption. Experimental studies using animal models have reported that microvibration stimulation improves bone quality in osteoporosis model mice [7] and promotes bone formation in bone defects [8]. However, the mechanism by which microvibration stimulation regulates bone metabolism remains unknown. The effective vibration conditions also vary from study to study, and at present there is no consensus on the most effective vibration conditions.

Raman spectroscopy is a noninvasive and quantitative measurement technique. By analyzing the spectra obtained from Raman spectroscopy, information such as molecular structure, crystal composition and crystallinity can be obtained. Raman spectroscopy has been used to

This study was presented at the Symposium on Biomedical Engineering 2023, Kumamoto, September, 2023.
Received on July 23, 2023; revised on October 30, 2023; accepted on November 18, 2023.

[*] Graduate School of Technology, Industrial and Social Sciences, Tokushima University, Tokushima, Japan.
[**] Institute of post-LED Photonics, Tokushima University, Tokushima, Japan.
[#] 2–1 Minami Josanjima, Tokushima, Tokushima 770–8506, Japan.
E-mail: katsuyas@tokushima-u.ac.jp

evaluate bone in osteoporosis and osteoarthritis [9, 10], as well as to evaluate substrate calcification in cultured cells [11–13]. In this study, we used Raman spectroscopy to observe the composition and calcification of the matrix produced by cultured osteoblasts . We also evaluated the effect of microvibration stimulation on the matrix. KUSA-A1 cells, a mesenchymal stem cell line, were induced to differentiate into osteoblasts and produce bone matrix. Three groups of cell cultures were prepared: no vibration group, 45-Hz vibration group, and 90-Hz vibration group. Raman spectroscopy was used to measure multiple points in the culture dish to evaluate the calcification of the entire dish. Raman mapping was also performed to evaluate the degree of phosphate crystallinity and mineral to matrix ratio in the calcified matrix.

2. Methods

2.1 Cell culture

In this study, we used KUSA-A1, a mesenchymal stem cell line. Cells [14] were preincubated in culture flasks containing α-MEM (Wako, Japan) supplemented with 10% fetal bovine serum (FBS) as the culture medium. The culture conditions were humidified air at 37℃ and 5% CO_2. A glass bottom dish with a grid (Iwaki, Japan) was used for seeding cells and observing substrate production. This glass bottom dish is printed with a grid with intervals of 150 μm, allowing fixed-point observation and evaluation at the same location on the dish. KUSA-A1 cells were cultured until sub-confluent and then seeded at a density of 2.0×10^5 cells/ml in a glass bottom dish. After seeding, the osteoblast differentiation induction medium was used. Osteogenic reagents (2.5 mM β-glycerophosphate, 10 nM dexamethasone, 50 μg/ml L-ascorbic acid) and 60 mg/l kanamycin sulfate, an antibiotic, were added to the α-MEM with 10% FBS.

In this experiment, osteoblast cultures were prepared under three conditions. The control group was cultured statically without vibration. The 45-Hz vibration group and 90-Hz vibration group were stimulated with micro-vibrations at 45 Hz and 90 Hz, respectively, for 30 min per day at an acceleration amplitude of 0.2 G. All three groups were cultured for days 7, 9, 11 and 14. After the prescribed incubation period, cell samples were fixed with 4% paraformaldehyde and used for observation. Raman spectroscopy measurements of the preparations were performed in a glass bottom dish filled with PBS.

2.2 Microvibration loading device

In this study, we developed an original microvibration stimulation loading device (**Fig. 1**) that can provide microvibration stimulation in a CO_2 incubator (**Fig. 2**). This device consists of an audio cone speaker unit (PW80K, Fostex, Japan) with the center cone removed and a jig attached to it. The jig is connected to a vibration plate, which excites horizontal vibration. The vibrating plate is supported by a flexible gel and can move freely in the horizontal direction. A glass bottom dish seeded with cells is fixed to the vibrating plate with double-sided tape.

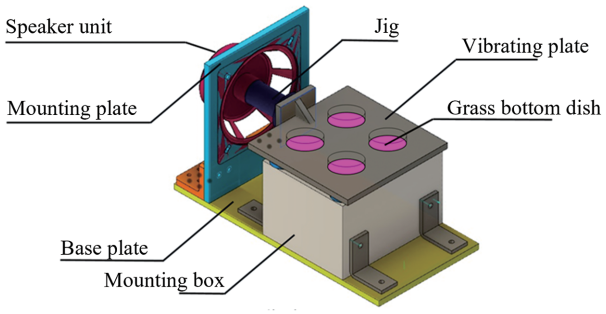

Fig. 1 CAD image of the microvibration loading device.

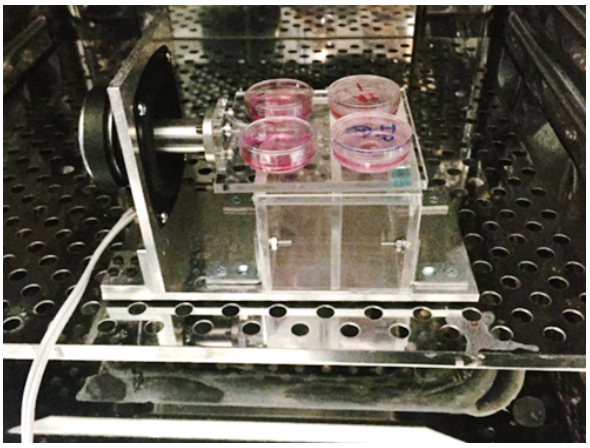

Fig. 2 Microvibration loading device in a CO_2 incubator.

Regarding the operation of the device, a sine wave voltage signal was output from a function generator (AG-253, Kenwood, Japan), and the signal was amplified by an audio amplifier (WP-C104, Panasonic, Japan) to drive a speaker. To test the operation of the device, a glass bottom dish filled with water as a dummy mass was fixed on top of the vibration plate, and an acceleration sensor was used to confirm that the specified acceleration amplitude and frequency were generated.

2.3 Phase contrast microscopy

A phase contrast microscope (CKX-41, Olympus, Japan) with dry 4× objective lens was used to observe the substrate produced by osteoblasts. A digital camera (DP-71, Olympus, Japan) was attached to the microscope to record the observed images. In the acquired phase contrast images, the areas of calcification of the matrix produced by osteoblasts were opaque and therefore appeared dark. Image J software (NIH, USA) was used to binarize the

images and measure the area of the darkened areas as calcified matrix. The acquired images were graded at 8 bits, and the binarization threshold was set at 124. This value is the average of the binarization thresholds of the acquired images according to Otsu's method [15]. The dark areas measured also included the grid drawn on the glass bottom dish. Therefore, the area of the grid alone was measured beforehand and subtracted to obtain the area of the calcified area.

2.4 Raman spectroscopy

A Raman microscope (Raman-11, Nanophoton, Japan) was used for Raman spectroscopy measurements. A 532 nm laser was used as the excitation light source. The objective lens was a water immersion 60× lens (N.A. 1.0). One pixel in an image acquired by Raman mapping corresponds to approximately 0.35 μm. Measurements were taken over the spectral range from 606.0 cm^{-1} to 1818.0 cm^{-1} with a spectral resolution of 1 cm^{-1}. The acquired data were analyzed using specialized software (Raman Viewer, Nanophoton, Japan). The acquired Raman spectrum had a peak at 958 cm^{-1} derived from hydroxyapatite, which is a substrate for matrix production by osteoblasts, and a peak at 950 cm^{-1} derived from Si-O contained in the glass. Therefore, we first obtained the spectrum of the glass bottom dish alone, and then performed pre-processing steps to subtract the spectrum. Other preprocessing steps were cosmic ray noise removal and smoothing, and baseline correction.

In this study, Raman spectroscopy measurements were performed using two different measurement methods: point measurement and Raman mapping. The measurement conditions for each method are described below.

In the point measurement, the laser power was 20.5 mW, the exposure time was 30 seconds, and the number of integration times was 2. Raman spectra were acquired at 20 random locations/dish. The acquired spectra were averaged and used for analysis. The spectra were normalized by the CH_2-derived peak (1447 cm^{-1}) for comparison of spectra among samples. The CH_2 peak in the Raman spectrum is derived from lipids and proteins as biomolecules. In the Raman spectra obtained in this experiment, the CH_2 peak showed the least variation and was almost constant in all groups of samples. Therefore, the CH_2 peak was used as a standard for comparing the peak height of the entire Raman spectrum.

For Raman mapping, a two-dimensional mapping of a 135.6 μm × 25.25 μm area was performed with a laser power of 20.6 mW and an exposure time of 10 seconds/line. Ten observation sites were randomly selected for each group. In the acquired Raman mapping image, the area with high Raman peak intensity for phosphate (958 cm^{-1}) was selected, and the Raman spectrum was acquired in the selected area measuring 2.4 μm × 2.4 μm (7 × 7 pixels). The acquired Raman spectra were averaged for analysis. In the analysis of Raman spectra, two indices were used: the mineral to matrix ratio and the degree of phosphate crystallinity. For the mineral to matrix ratio, we calculated the peak intensity ratio between the phosphate (958 cm^{-1}) peak and the amide 1 band (1600 – 1700 cm^{-1}), which is considered to be derived from protein. Amide 1 is a bond found in a variety of proteins, but in this study, it was used specifically to evaluate the mineral to matrix ratio in osteoblastogenic substrates, as it reflects the secondary structure of collagen. Sub-band curve fitting was also performed to evaluate the crystallinity of the phosphate. The inverse of the full width at half maximum was calculated for the obtained phosphate sub-bands and used as an index of crystallinity [16, 17].

2.5 Statistical analysis

One-way analysis of variance (ANOVA) was used for statistical analysis, followed by Tukey's method for multiple comparison tests. All data are expressed as mean ± standard deviation. The statistical significance level was set at $P < 0.05$, and significant differences are indicated by * in the graphs.

3. Results

3.1 Phase contrast microscopy

Figures 3, 4 and 5 show the phase contrast images of the control, 45-Hz vibration and 90-Hz vibration groups, respectively, on days 7, 9, 11 and 14. In each group, the area of the calcified area (which appears white or light brown in the phase contrast images, while the glass surface appears to be dark bluish gray) increased with increase in number of days of incubation. The phase con-

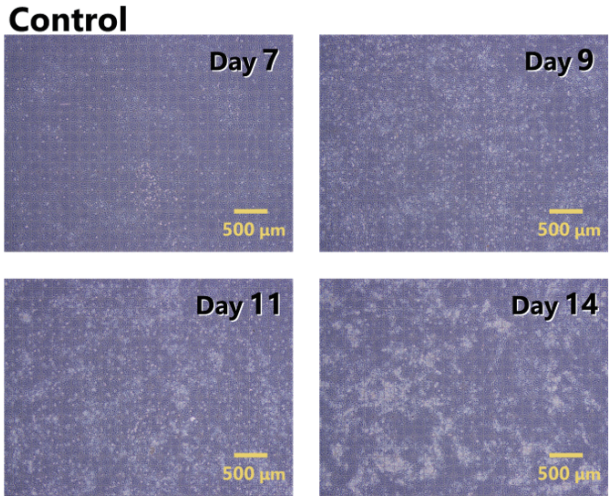

Fig. 3 Phase contrast images for the four incubation periods in the control group.

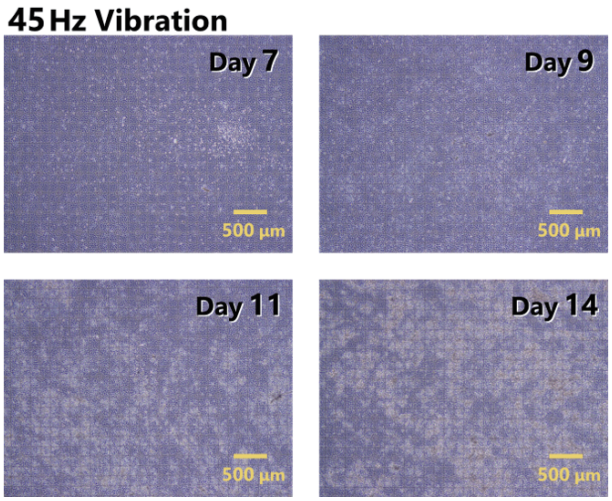

Fig. 4 Phase contrast images for the four incubation periods in the 45-Hz vibration group.

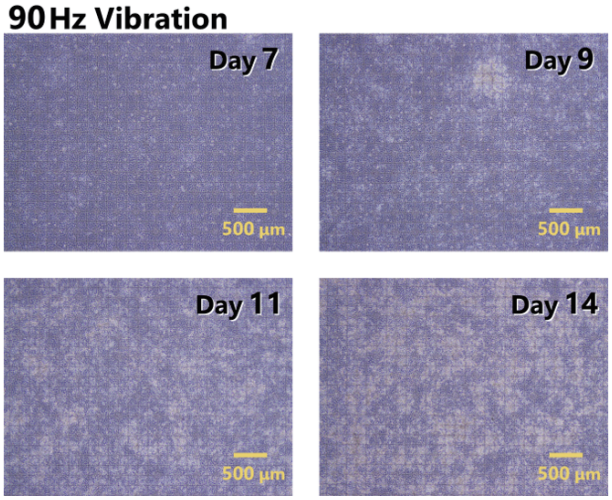

Fig. 5 Phase contrast images for the four incubation periods in the 90-Hz vibration group.

trast images on the 14th day of incubation were binarized (**Figure 6**, corresponding to images of day 14 in **Figs. 3–5**), and the areas of the calcified areas were measured. The images are pseudo-colored, with light areas shown in light blue and dark areas in red. **Table 1** shows the percentage of calcified areas obtained from the measurements. The 90-Hz vibration group had the largest area of calcification, followed by the 45-Hz vibration group. The area of calcified area in the control group was smaller than those in the microvibration groups.

3.2 Raman spectroscopy point measurement

The results of point measurements by Raman spectroscopy are described. **Figures 7, 8 and 9** show the average Raman spectra obtained from measurements at 20 points in each group, offset by the incubation period. In each group, the phosphate peak (957 cm^{-1}) gradually increased as the incubation period lengthened. **Figure 10**

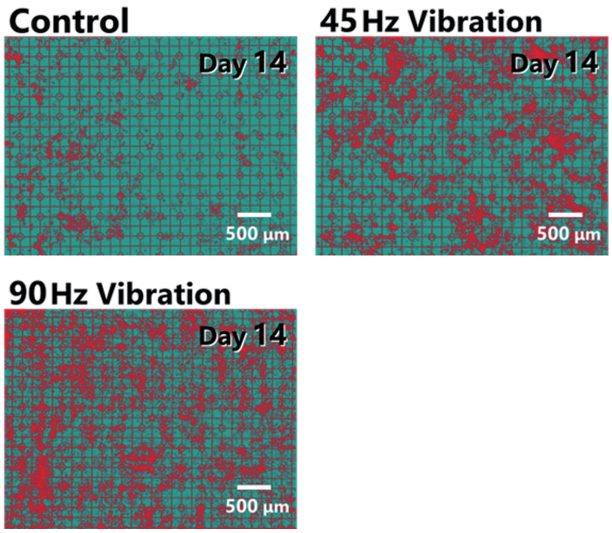

Fig. 6 Binarized phase contrast images at day 14 of the incubation period, with calcified areas displayed in pseudo-color.

Table 1 Percentage of calcified areas measured from phase-contrast observation images.

	Percentage of calcified area [%]
Control	1.17
45 Hz vibration	15.76
90 Hz vibration	21.99

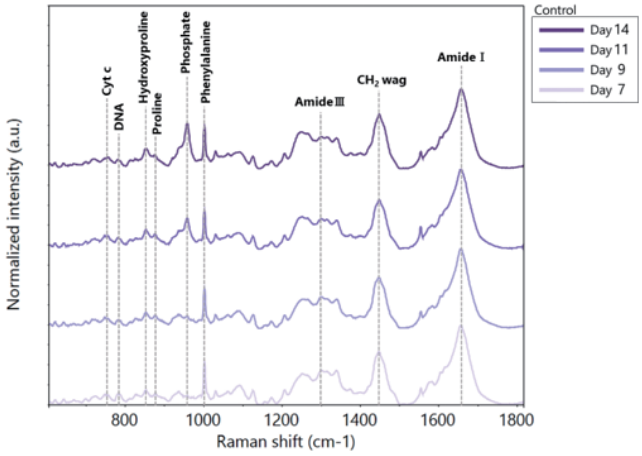

Fig. 7 Raman spectra for the four incubation periods in the control group.

shows enlarged average Raman spectra around the phosphate peak of each group on the 14th day of incubation. The 45-Hz vibration group showed the highest peak height, followed by the control group, and the 90-Hz vibration group had the lowest peak height.

3.3 Raman spectroscopy Raman mapping

Next, the measurement results of Raman mapping are

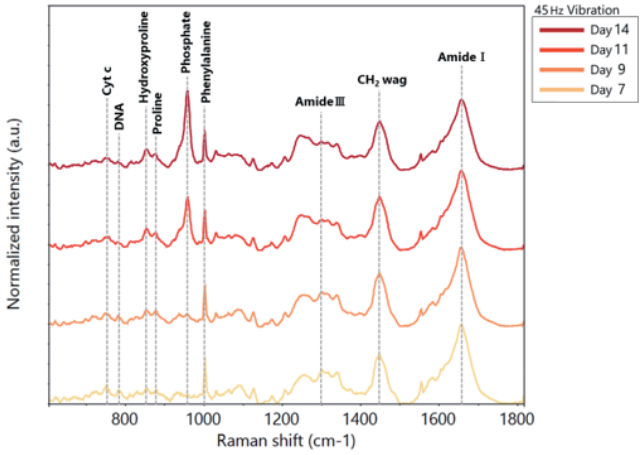

Fig. 8 Raman spectra for the four incubation periods in the 45-Hz vibration group.

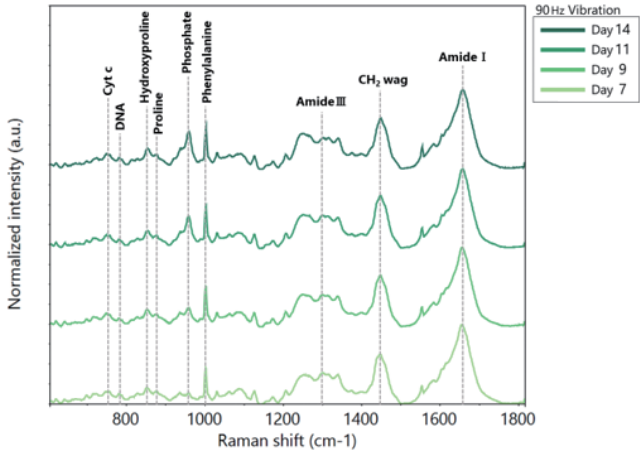

Fig. 9 Raman spectra for the four incubation periods in the 90-Hz vibration group.

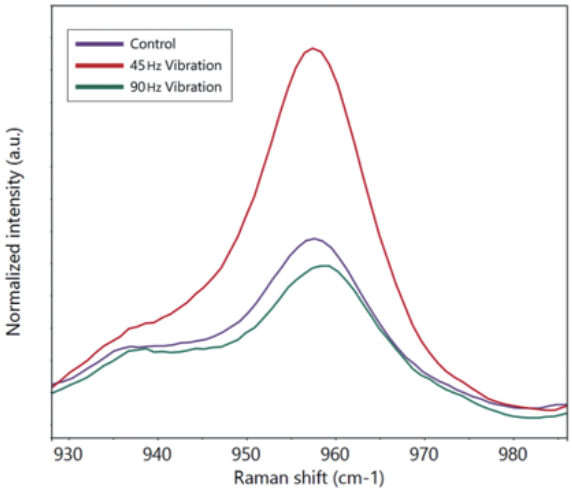

Fig. 10 Enlarged Raman spectra of the three groups at day 14 of incubation, with bands near the phosphate peak.

described. **Figure 11** shows an example of a phase contrast image and an image mapping the signal intensity of the phosphate peak (958 cm^{-1}) at that location. As shown in the figure, there is a distribution of the Raman signal intensity of phosphate even in the opaque region (calcified region) in the phase contrast image. **Figure 12** shows the average Raman spectra obtained by selecting locations with high Raman signal intensity for phosphate among the 10 Raman mappings obtained for each group. The obtained Raman spectra were analyzed for mineral to matrix ratio (phosphate/amide 1) and phosphate crystallinity. **Figures 13 and 14** show the measurements and results of mineral to matrix ratios for the three groups on day 14 of incubation. The mineral to matrix ratio was highest in the 90-Hz vibration group and tended to be lower in the 45-Hz vibration group and the control group, but the differences were not statistically signifi-

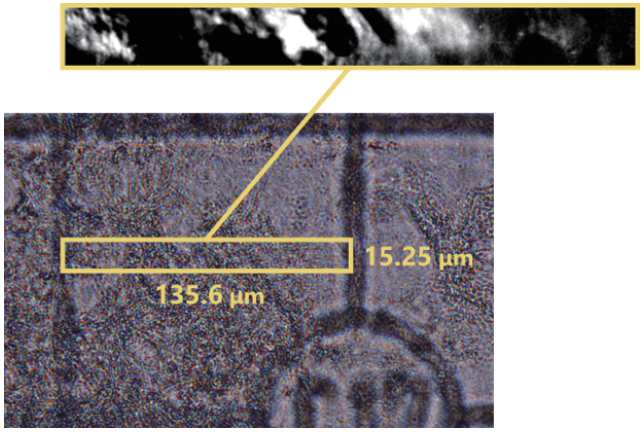

Fig. 11 An example of phase contrast image and Raman mapping of a part of the image. X-Y mapping of the signal intensity of the phosphate peak is shown.

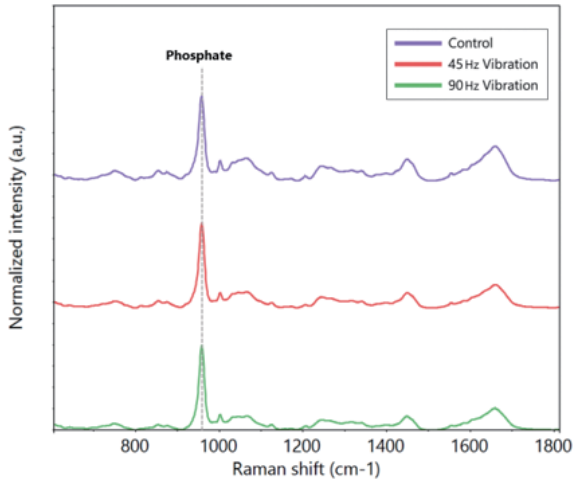

Fig. 12 Raman spectrum obtained by selecting areas with high signal intensity of phosphate peaks from the image obtained by Raman mapping. The incubation period was 14 days, and the spectra of the three groups are offset.

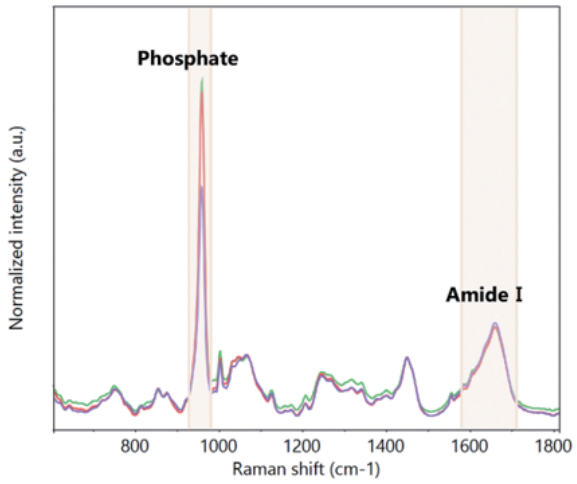

Fig. 13 Graph showing the phosphate peak and the amide 1 peak used to calculate the mineral to matrix ratio on the Raman spectrum.

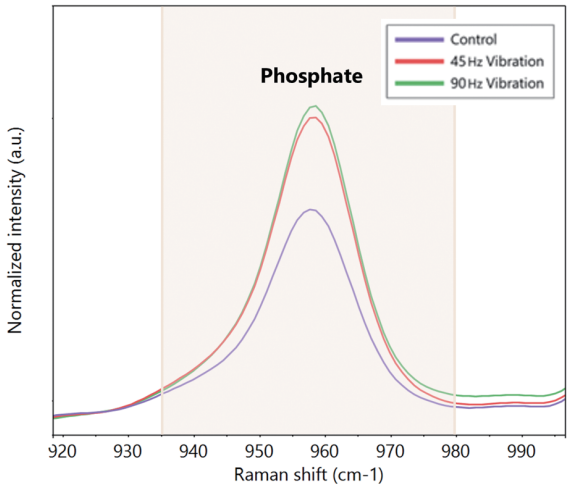

Fig. 15 Graph of Raman spectra magnified near the phosphate peak used to calculate the crystallinity of phosphate.

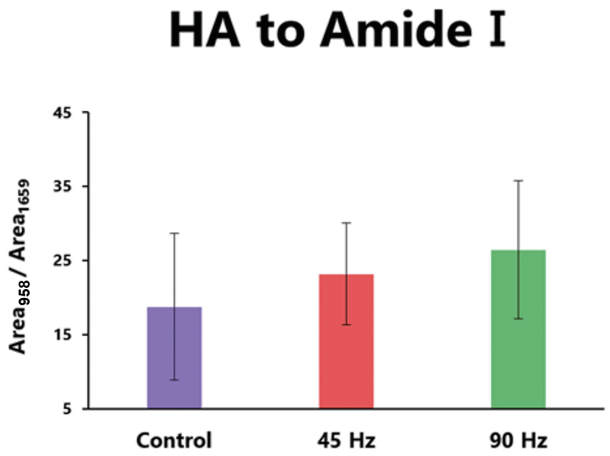

Fig. 14 Comparison of mineral to matrix ratios in the three groups, incubation period was 14 days.

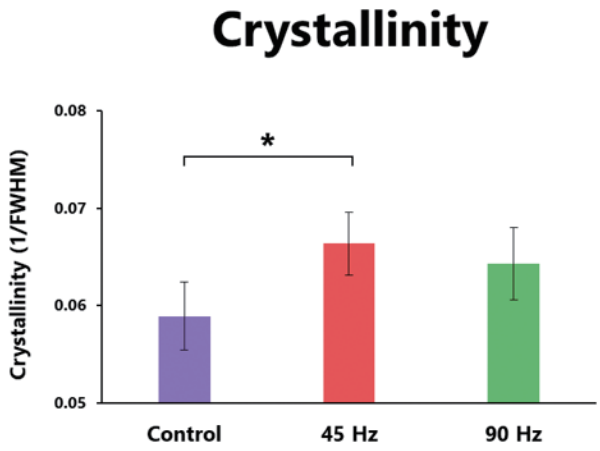

Fig. 16 Comparison of phosphate crystallinity, incubation period is 14 days.

cant. **Figure 15** shows the magnified Raman spectra for the phosphate peak used to calculate crystallinity of phosphate, and **Fig. 16** is a plot of the inverse of the full width at half maximum of the phosphate band calculated to evaluate the crystallinity of phosphate. There was a statistically significant difference in crystallinity only between the control group and the 45-Hz vibration group. Hence, the degree of crystallinity tended to increase in the group that received microvibration stimulation.

4. Discussion

Phase contrast microscopy revealed that the amount of substrate produced by microvibration-stimulated osteoblasts increased in both the 45-Hz and 90-Hz vibration groups. Bone metabolism is regulated by hormones and cytokines *in vivo*, as illustrated by the fact that osteoporosis is caused by estrogen deficiency. The mechanism by which microvibration stimulation activates bone metabolism may be regulation by sensing mechanical stress in tissues and organs other than bone and secretion of bone metabolism factors. However, as shown by the results of this study, substrate production increased even when microvibration stimulation was applied to cultured osteoblasts. This result suggests that osteoblasts per se possess mechanisms to respond to microvibration stimulation and upregulate their own osteogenic activity.

In the phase contrast images, the area of opaque regions (presumably calcified regions) was the largest in the 90-Hz vibration group. On the other hand, Raman spectroscopy point measurements showed that the 45-Hz vibration group had the highest peak signal intensity of the phosphate band, while the 90-Hz vibration group had a lower peak intensity than the control group. One possible reason for these findings is that 90-Hz microvibration stimulation upregulates substrate production by osteo-

blasts, but the phosphate in the substrate produced may be immature. In point measurements, measurements were made at 20 random points on the glass bottom dish, and the spectra obtained were averaged and evaluated. Therefore, the areas that were counted as opaque areas in the phase contrast image may have contained large amounts of substrate composed of very immature phosphate. Compared to the 90-Hz vibration group, the 45-Hz vibration group showed more substrate production and higher Raman peak intensity of phosphate in both phase contrast imaging and Raman spectroscopy.

Next, the results of the analysis of the spectra obtained from the Raman spectroscopy mapping images are discussed. The mineral to matrix ratio was highest in the 90-Hz vibration group, and the ratio in the 45-Hz vibration group also tended to be higher than the control group, but none of the differences were statistically significant. In the Raman mapping measurement, spectra were obtained by selecting areas with high Raman peak intensities of phosphate in the mapping images. Calcification of the substrate produced by osteoblasts does not proceed uniformly throughout, but is heterogeneous. However, Raman mapping selects the most calcified areas in each group. As a result, there may not be much difference among the three groups. In this sense, microvibration stimulation increases osteoblast substrate production and promotes calcification, but may have little effect on the composition of substrate in the calcified area, as reflected by the mineral to matrix ratio.

Subsequently, we discuss the crystallinity results obtained from the Raman mapping measurements. The highest crystallinity of phosphate was observed in the 45-Hz vibration group, with a statistically significant difference compared to the control group; the 90-Hz vibration group also showed a trend toward higher crystallinity, although the difference was not statistically significant. These results suggest that microvibration stimulation may have an effect on the calcification of osteoblast-produced substrates to produce more mature and crystalline substrates. This suggests that microvibration stimulation may have both quantitative and qualitative effects on osteoblast substrate production, which is very useful for the practical application of microvibration stimulation to promote artificial bone formation.

The results of the experiments in this study showed that microvibration stimulation increased osteoblast substrate production and promoted calcification. In particular, 45-Hz vibration had potent promoting effects on the amount of substrate production, Raman peak intensity of phosphate, and crystallinity. Although comparisons were made for only two different frequencies, it is clear that different frequencies of microvibration stimulation have very different effects on osteoblast substrate production. In the future, it is necessary to clarify the effects of microvibration stimulation for a wider range of frequencies. Furthermore, the vibration conditions of microvibration stimulation include not only frequency but also a wide variety of parameters such as vibration intensity, duration of stimulation, number of times of stimulation, and pause period. Among these very diverse combinations of many parameters, the search for the optimal combination to promote bone formation is not easy. This is especially true for animal models that require long experimental periods and experimental resources. Therefore, it is useful to use a simplified *in vitro* experimental system of cell cultures to search for optimal stimulation parameters.

5. Conclusion

In this study, osteoblasts were cultured under microvibration stimulation, and substrate production was evaluated by phase contrast microscopy and Raman spectroscopy. The results obtained from phase contrast images showed that substrate production by osteoblasts increased when microvibration was applied, and the highest substrate production was observed in the 90-Hz vibration group. The Raman spectroscopy point measurements showed the highest Raman peak intensity of phosphate in the 45-Hz vibration group, whereas the peak intensity in the 90-Hz vibration group was lower than that in the control group. These results suggest that 90-Hz vibration stimulation increases substrate production by osteoblasts, but the substrate produced may be immature. Spectral measurements based on Raman mapping showed that microvibration stimulation, especially at 45 Hz, had the effect of increasing crystallinity of phosphate in the substrate produced by osteoblasts.

Acknowledgement

The authors would like to thank Mr. Hirofumi Hosokawa for his invaluable assistance in conducting the experiments and analysis.

References

1. Kanis JA: Assessment of fracture risk and its application to screening for postmenopausal osteoporosis: synopsis of a WHO report. Osteoporos Int. **4**(6), 368–381, 1994.
2. Browner WS, Pressman AR, Nevitt MC, Cummings SR: Mortality following fractures in older women: the study of osteoporotic fractures. Arch Intern Med. **156**(14), 1521–1525, 1996.
3. Forsén L, Sogaard AJ, Meyer HE, Edna T, Kopjar B: Survival after hip fracture: short- and long-term excess mortality according to age and gender. Osteoporos Int. **10**(1), 73–78, 1999.
4. Yager JD, Davidson NE: Estrogen carcinogenesis in breast cancer. N Engl J Med. **354**(3), 270–282, 2006.
5. Gonzalez-Moles MA, Bagan-Sebastian JV: Alendronate-related oral mucosa ulcerations. J Oral Pathol Med. **29**(10), 514–518,

2000.

6. Rubin CT, McLeod KJ: Promotion of bony ingrowth by frequency-specific, low-amplitude mechanical strain. Clin Orthop Relat Res. **298**, 165–174, 1994.
7. Tezval M, Biblis M, Sehmisch S, Schmelz U, Kolios L, Rack T, Stuermer KM, Stuermer EK: Improvement of femoral bone quality after low-magnitude, high-frequency mechanical stimulation in the ovariectomized rat as an osteopenia model. Calcif Tissue Int. **88**(1), 33–40, 2011.
8. Matsumoto T, Goto D: Effect of low-intensity whole-body vibration on bone defect repair and associated vascularization in mice. Med Biol Eng Comput. **55**(12), 2257–2266, 2017.
9. Orkoula MG, Vardaki MZ, Kontoyannis CG: Study of bone matrix changes induced by osteoporosis in rat tibia using Raman spectroscopy. Vibrational Spectroscopy. **63**, 404–408, 2012.
10. Nieuwoudt MK, Shahlori R, Naot D, Patel R, Holtkamp H, Aguergaray C, Watson M, Musson D, Brown C, Dalbeth N, Cornish J, Simpson MC: Raman spectroscopy reveals age and sex related differences in cortical bone from people with osteoarthritis. Sci Rep. **10**(1), 1–14, 2020.
11. Stewart S, Shea DA, Tarnowski CP, Morris MD, Wang D, Franceschi R, Lin D-L, Keller E: Trends in early mineralization of murine calvarial osteoblastic cultures: a Raman microscopic study. J Raman Spectroscopy. **33**(7), 536–543, 2002.
12. Smith SJ, Emery R, Pitsillides A, Clarkin CE, Mahajan S: Detection of early osteogenic commitment in primary cells using Raman spectroscopy. Analyst. **142**(11), 1962–1973, 2017.
13. Bouzy P, O'Grady S, Madupalli H, Tecklenburg M, Rogers K, Palombo F, Morgan MP, Stone N: A time-course Raman spectroscopic analysis of spontaneous in vitro microcalcifications in a breast cancer cell line. Lab Invest. **101**(9), 1267–1280, 2021.
14. Umezawa A, Maruyama T, Segawa K, Shadduck RK, Waheed A, Hata J: Multipotent marrow stromal cell line is able to induce hematopoiesis in vivo. J Cell Physiol. **151**(1), 197–205, 1992.
15. Otsu N: A Threshold Selection Method from Gray-Level Histograms. IEEE Trans Syst Man Cybernetics. **9**(1), 62–66, 1979.
16. Mandair GS, Morris MD: Contributions of Raman spectroscopy to the understanding of bone strength. BoneKEy Rep. **4**, 620, 2015.
17. Brauchele E, Berrio DC, Rieger M, Schenke-Layland K, Reinert S, Alecander D: Raman spectroscopic analyses of jaw periosteal cell mineralization. Stem Cells Int. 2017, 1651376, 2017.

Katsuya Sato

Katsuya Sato has received the B.E., M.E. and D.E. degrees from Kobe University in 2000, 2002 and 2005, respectively. He has worked at Yamaguchi University as an assistant professor from 2005 to 2009. Since 2009, he has been an associate professor at Tokushima University. His current research interests are cell biomechanics, mechanobiology, MEMS and Bioengineering. He is a member of Japan Society of Mechanical Engineers, Japanese Society for Medical and Biological Engineering, Japanese Society for Bone Morphometry and the Biophysical Society of Japan.

Takeo Minamikawa

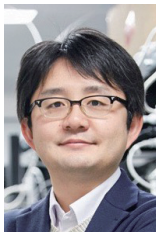

Takeo Minamikawa received his B.E., M.E., and Ph.D. from Osaka University, Japan, in 2006, 2008, and 2010, respectively. He was a JSPS Research Fellowship for Young Scientists from 2011 to 2013 and served as an Assistant Professor and Visiting Associate Professor at Kyoto Prefectural University of Medicine from 2013 to the present. From 2017 to 2021, he was also a PRESTO researcher at Japan Science and Technology Agency. He is currently an Associate Professor at Tokushima University, Japan, a Visiting Director at National Cerebral and Cardiovascular Center, and a Visiting Associate Professor at Kyoto Prefectural University of Medicine. His research interests include Raman spectroscopy, nonlinear photonics, plasmonics, optical-frequency-comb spectroscopy, and their medical and biological applications. Members of the Japan Society of Mechanical Engineers, the Japan Society of Applied Physics, the Optical Society of Japan, the Spectroscopical Society of Japan, the Laser Society of Japan, the Japan Society of Hepatology, Kyoto Foundation for the Promotion of Medical Science, the Japan Society for Laser Microscopy, the Optical Society of America (OPTICA) and the International Society for Optics and Photonics (SPIE).

Takeshi Yasui

Takeshi Yasui received the first Ph.D. degree in engineering from the University of Tokushima, Tokushima, Japan, in 1997 and the second Ph.D. degree in medical science from the Nara Medical University, Yagi, Japan, in 2013. From 1997 to 1999, he was a Postdoctoral Research Fellow with the National Research Laboratory of Metrology, Tokyo, Japan. From 1999 to 2010, he was with the Graduate School of Engineering Science, Osaka University, Suita, Japan. He is currently a Chief Research Officer (CRO) and a Professor with the Institute of Post-LED Photonics, Tokushima University. His research interests include biomedical optics, THz optics, and optical frequency comb. He is a Member of the Optical Society, the International Society for Optical Engineering, the Japan Society of Applied Physics, the Optical Society of Japan, the Laser Society of Japan, the Japanese Society for Medical and Biological Engineering, and the Japan Society of Mechanical Engineers.